REVIEW OF HIGH CYCLE FATIGUE MODELS APPLIED FOR MULTIAXIAL TENSION-TORSION LOADING BASED ON A NEW ACCURACY ASSESSMENT PARAMETER

KUN LORAND[1, 2*]

[1] *"Politehnica" University of Timisoara, Mechanical Engineering Faculty, Department of Mechanics and Strength of Materials, Bv. Mihai Viteazul 1, Timisoara, 300222, Romania*

[2] *National R&D Institute for Welding and Material Testing – ISIM Timisoara, Bv. Mihai Viteazul 30, Timisoara, 300222, Romania*

Abstract: A parameter denoted "Critical Position Offset Angle" – CPOA is proposed in this paper, developed as a new approach for assessing the accuracy of multiaxial HCF models based on the angle difference between the predicted critical plane and the plane where the equivalent stress reaches its peak value. A number of 11 models are compared using this parameter, by applying them to simulated multiaxial tension-torsion loadings with different grades of nonproportionality. A wider scatter in CPOA values is identified in cases of loading with dominant shear stress. Overall, the equivalent stress models give the best results.

Keywords: critical position offset angle, HCF, multiaxial, fatigue model, equivalent stress, critical plane, stress invariant, phase angle

1. INTRODUCTION

Correct assessment of multiaxial fatigue damage constitutes an unresolved problem for the engineering community ever since the first fatigue studies had been published. Engineering calculations involve many times the reduction of a complex multiaxial state of stress into an equivalent uniaxial one, without verifying the validity of the reduction criteria for the given load case, material and piece geometry.

Fatigue calculation has become an important part of machine design. However, multiaxial fatigue remains a domain approached by a limited number of specialists. Although in recent years Low Cycle Fatigue (LCF) has gained the most attention, studies are still made in the field of High Cycle Fatigue (HCF) too. New research is needed in the field of HCF since many components from industries with strategic importance (such as nuclear [1]) are operating in the HCF domain and early or unexpected failures can have catastrophic consequences claiming human lives.

Several review papers have been published concerning the applicability of multiaxial fatigue models, based on different considerations. Some authors present the models in a critical manner [2, 3, 4], while others confront them with experimental data and assess their accuracy [1, 5, 6].

This paper aims to put into a new light eleven of the most often used multiaxial HCF models, by applying them to mathematically simulated proportional and nonproportional tension-torsion loading cases and assessing them

* Corresponding author, email: kunlori@yahoo.com

based on the influence of two parameters: the predicted equivalent stress and the "critical position offset angle" (CPOA) between the predicted critical plane and the plane where the equivalent stress reaches its peak value, both as functions of the phase shift angle and stress cycle amplitudes.

2. REVIEW OF SELECTED HCF MODELS

The study presented in this paper is concerned in analyzing multiaxial HCF models widely used in machine design for their relative simplicity and acceptable accuracy in predicting fatigue life. The following list is not comprehensive, since many other types of HCF models exist, but lack practical utility because they require high level mathematical knowledge to apply [4]. The selected models for this study are the following [3]:

- Equivalent stress models: von Mises [7], "signed von Mises" [8], Tresca [9], Sines [10];
- Critical plane models: Yokobori [11], Findley [12], Matake [13], McDiarmid [14];
- Models based on stress invariants: Crossland [15], Sines (II) [16], Kakuno-Kawada [17].

The mentioned models differ significantly in terms of interpretation of the three-dimensional stress state, but they are all applicable for multiaxial loadings and are used in engineering calculations. They are briefly summarized in Table 1.

Table 1. Main parameters of selected HCF damage models.

No	Model	Damage Parameter (DP)	Failure predicted, if:	Critical plane	Applicable for prop./ nonprop.
1	von Mises	$\frac{1}{\sqrt{2}}\sqrt{(\sigma_x-\sigma_y)^2+(\sigma_y-\sigma_z)^2+(\sigma_z-\sigma_x)^2+6(\tau_{xy}^2+\tau_{yz}^2+\tau_{zx}^2)}$	$(DP) > \tau_{-1}$	$\tau_{oct}\ max$	Yes / Yes
2	Signed von Mises	$sign(\sigma_1)\cdot\sigma_{vM}$	$(DP) > \tau_{-1}$	$\tau_{oct}\ max$	Yes / Yes
3	Tresca	$\sigma_3 - \sigma_1$	$(DP) > \tau_{-1}$	$\tau_{oct}\ max$	Yes / Yes
4	Sines	$\frac{\Delta\tau_{oct}}{2}+\left[\frac{\frac{2\sqrt{2}}{3}\left(\sigma_{-1}-\frac{\sigma_0}{2}\right)}{\sigma_0}\right]\cdot 3\sigma_h$	$(DP) > \frac{\sqrt{3}}{2}\sigma_{-1}$	$\tau_{oct}\ max$	Yes / No
5	Yokobori	$\tau_n+\frac{2\tau_{-1}}{\sigma_{-1}}\sigma_n$	$(DP) > \tau_{-1}$	$\tau\ max$	Yes / Yes
6	Findley	$\frac{\Delta\tau}{2}+\left(\frac{2\tau_{-1}}{\sigma_{-1}}-1\right)\sigma_n$	$(DP) > \tau_{-1}$	$\left[\frac{\Delta\tau}{2}+\left(\frac{2\tau_{-1}}{\sigma_{-1}}-1\right)\sigma_n\right]max$	Yes / Yes
7	Matake	$\frac{\Delta\tau}{2}+\left(\frac{2\tau_{-1}}{\sigma_{-1}}-1\right)\sigma_n$	$(DP) > \tau_{-1}$	$\frac{\Delta\tau}{2}\ max$	Yes / Yes
8	McDiarmid	$\frac{\Delta\tau}{2}+\left(\frac{2\tau_{-1}}{\sigma_{UTS}}\right)\sigma_n$	$(DP) > \tau_{-1}$	$\frac{\Delta\tau}{2}\ max$	Yes / Yes
9	Crossland	$\sqrt{J_{2a}}+\left(\frac{3\tau_{-1}}{\sigma_{-1}}-\sqrt{3}\right)\cdot\sigma_{h,max}$	$(DP) > \tau_{-1}$	$\frac{\Delta\tau_{oct}}{2}\ max$	Yes / Yes
10	Sines (II)	$\sqrt{J_{2a}}+\left(\frac{3\tau_{-1}}{\sigma_0}-\sqrt{3}\right)\cdot\sigma_{h,m}$	$(DP) > \tau_{-1}$	$\frac{\Delta\tau_{oct}}{2}\ max$	Yes / Yes
11	Kakuno-Kawada	$\sqrt{J_{2a}}+\left(\frac{3\tau_{-1}}{\sigma_{-1}}-\sqrt{3}\right)\cdot\sigma_{h,m}+\left(\frac{3\tau_{-1}}{\sigma_0}-\sqrt{3}\right)\cdot\sigma_{h,a}$	$(DP) > \tau_{-1}$	$\frac{\Delta\tau_{oct}}{2}\ max$	Yes / Yes

where: σ_x, σ_y, σ_z, τ_{xy}, τ_{yz}, τ_{zx} – components of the stress tensor;
σ_1, σ_3 – principal normal stresses;
τ_{oct} – octahedral shear stress;
σ_n – normal stress acting on plane *n*;
J_{2a} – amplitude of the second invariant of the deviatoric stress tensor;
σ_h – hydrostatic stress;
σ_{UTS} – ultimate tensile stress;
σ_{-1} – fatigue limit under fully reversed tension-compression (R = -1);
σ_0 – fatigue limit under repeated tension (R = 0);
τ_{-1} – fatigue limit under fully reversed torsion (R = -1);
Other: m – mean; a – amplitude; Δ – range.

The equivalent stress models start from the six-component stress tensor and generate one equivalent component, thus transforming general multiaxial stress state into an equivalent uniaxial one. This comes as a disadvantage, since the effect of loading direction is eliminated. However, these models are the most widely applied due to their simplicity and generally conservative predictions. These models also have limitations, such as in the case of the von Mises theory [7], which always produces a positive tension load cycle, eliminating the compressive components. The "signed von Mises" model [8] corrects this, but it requires the determination of the principal stresses, which complicates the calculations. The application of the Tresca model [9] can also come with some difficulty, due to the necessity of solving a cubic equation in order to find the three principal stresses. As for the Sines criterion [10], which can also be considered a critical plane model, is defined only for proportional loading, Sines did not give any solutions for nonproportionality.

The critical plane models are based on a different idea, stating that fatigue damage accumulates on a specific plane in the material, denoted the "critical plane". The damage parameter is a linear combination of shear stress and normal stress, acting on the critical plane. If applied correctly, these models are usually less conservative than the equivalent stress models. However, the determination of the critical plane often poses difficulties for the specialists. While Yokobori [11] considers the critical plane to be one along which the shear stress reaches an extreme value, Findley [12] proposes that the linear combination of shear stress amplitude and normal stress define the critical plane. Matake [13] and McDiarmid [14] consider that the maximum shear stress amplitude defines the plane where fatigue damage first appears. Given the differences in defining the governing parameters, much attention is needed in applying critical plane models.

The models based on stress invariants correlate fatigue life with the second invariant (J_2) of the deviatoric stress tensor. Since J_2 is related to the octahedral shear stress, according to the stress invariant models fatigue damage will occur on the octahedral plane, i.e. on the plane where the octahedral shear stress reaches its peak value. Thus, all three selected models consider a damage parameter defined as a linear combination of the square root of J_2 amplitude and the hydrostatic stress. The Crossland [15], Sines (II) [16] and Kakuno-Kawada [17] models differ from each other in defining the hydrostatic part of the equivalent stress. These models are generally in good correlation with experimental data, however the calculation of J_2 can prove to be extremely laborious and inconsistent in case of nonproportional loading.

3. DETERMINATION METHOD FOR CPOA

The used calculation methods will be presented in this paragraph, structured as follows: definition of the original load spectrum, transformation of the original load spectrum into a state of plane stress, finding of the critical time moment on the load cycle, definition of the analyzed load cases with different grades of nonproportionality, calculation of representative stresses followed by calculation of equivalent stresses according to the presented models. The mathematical part was realized with a program especially written for this purpose, in MathCad environment.

3.1. Definition of CPOA

As stated before, the Critical Position Offset Angle – CPOA represents the mathematical difference between the position angle of the plane where the considered equivalent stress reaches its peak value – $\theta_{\sigma eq}$ and the position angle of the critical plane – θ_{cp}, both angles as predicted by the corresponding HCF model. The mathematical expression of CPOA is the following:

$$CPOA = \left| \theta_{\sigma_{eq}} - \theta_{cp} \right| \tag{1}$$

The idea behind CPOA is that the plane where the equivalent stress is maximum should coincide with the plane predicted as critical by the corresponding HCF model. As a result of this, according to an assessment based on CPOA, a given model is the better defined the lower the value of CPOA is. As an example, if CPOA is zero, the model is considered to be well defined, and as CPOA increases, the model loses in accuracy.

3.2. Transformation of general stress state into plane stress and finding the representative time moment on the load cycle

The starting point of the present study is a general six-component stress history, based on the loading studied in another work [18]. However, this time constant amplitude stress histories are used, as presented in Figure 1, where a sequence of 5 full cycles are plotted. The general equation for each of the six stress components is the following:

$$\sigma(t) = \sigma_m + \sigma_a \cdot sin(\omega t + \Phi) \tag{2}$$

where Φ is the phase shift angle, the parameter which defines the grade of nonproportionality in the present study.

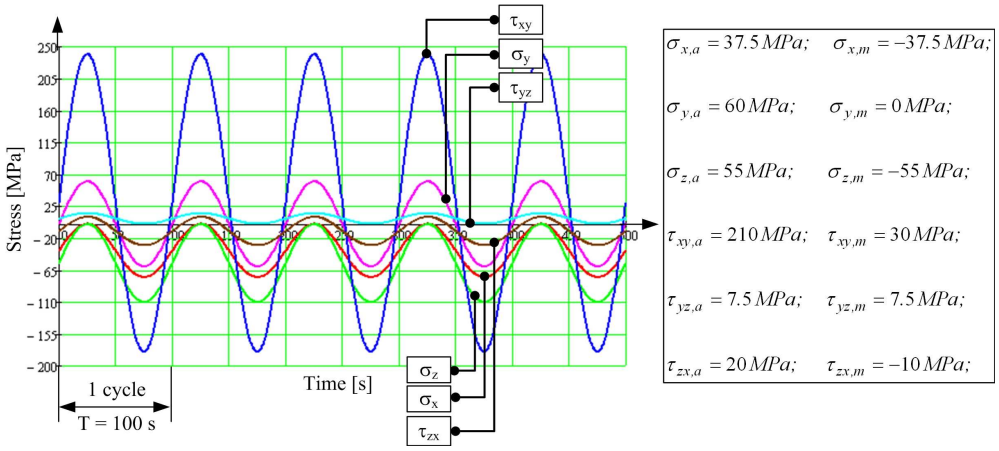

Fig. 1. Original three-dimensional proportional (Φ = 0) stress history and component means and amplitudes.

In order to simplify the calculations and to ease visualization, the complex stress history presented in Figure 1 was decomposed into three cases of plane stress. The decomposed load histories, plotted in σ-τ coordinates, are given in Figure 2 a, b and c.

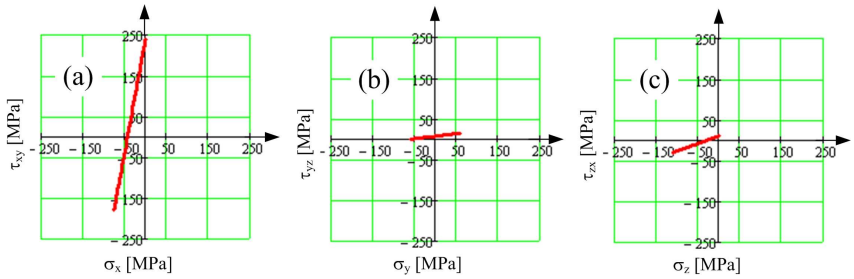

Fig. 2. Decomposed stress history in 3 states of plane stress.

A very important phase in the processing of the load spectrum is the determination of the most representative time moment on the cycle. The criterion of the worst possible case is applied, meaning the time moment exhibiting the highest stress values is chosen for further analysis. In order to account for the possibility of nonproportional loading, the critical time moment is defined as the moment at which the corresponding point on the σ-τ graph in Figure 2 is at the highest distance from the origin of the coordinate system.

It can be clearly seen that the highest distance from the 3 graphs in Figure 2a, b and c is reached in Figure 2a. The highest distance and the time moment at which it is reached on the 100 s long cycle are automatically determined by an algorithm especially written for this purpose in MathCad environment (Figure 3).

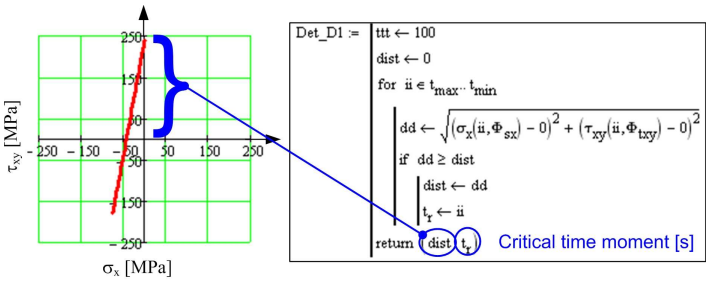

Fig. 3. Calculation of the highest distance (dist) on the loading path from the origin and the corresponding time moment (t_r).

3.3. Loading cases considered for the analysis

The original load spectrum and thus the loading case presented in Figure 3 are proportional. Since one objective of this study is to analyze the influence of nonproportionality on the applicability of different HCF models, the loading case in Figure 3 has been altered in terms of phase shift angle and stress amplitudes. As a result of this, a number of 14 different loading cases are subjected to analysis in this paper, as presented in Table 2.

Table 2. Analyzed loading cases.

No	Cycle definition parameters					dist [MPa]	t_r [s]	Loading path
	σ_a [MPa]	σ_m [MPa]	τ_a [MPa]	τ_m [MPa]	Φ [deg]			
A1	37.5	-37.5	210	30	0	240	25	proportional
A2	37.5	-37.5	210	30	15	240	21	nonproportional
A3	37.5	-37.5	210	30	30	240	17	nonproportional
A4	37.5	-37.5	210	30	45	240	12	nonproportional
A5	37.5	-37.5	210	30	60	241	8	nonproportional
A6	37.5	-37.5	210	30	75	242	4	nonproportional
A7	37.5	-37.5	210	30	90	243	0	nonproportional
B1	210	30	37.5	-37.5	0	240	25	proportional
B2	210	30	37.5	-37.5	15	240	25	nonproportional
B3	210	30	37.5	-37.5	30	240	25	nonproportional
B4	210	30	37.5	-37.5	45	240	25	nonproportional
B5	210	30	37.5	-37.5	60	241	25	nonproportional
B6	210	30	37.5	-37.5	75	242	25	nonproportional
B7	210	30	37.5	-37.5	90	243	25	nonproportional

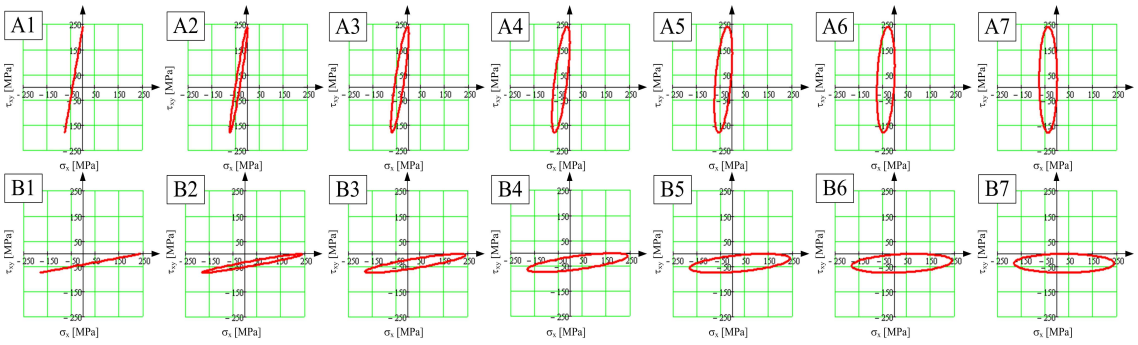

Fig. 4. Analyzed loading cases plotted in σ-τ coordinates.

3.4. Calculation of representative stress histories as functions of plane angle

In order to be able to apply the HCF models presented in Table 1, the magnitudes and directions of several quantities of interest need to be known:

- position of the planes along which the stresses σ, τ and τ_{oct} reach their maximum in t_r and their values;
- position of the planes along which the principal stresses σ_1, σ_2, τ_{12} reach their maximum in t_r and their values;

- position of the planes along which the stress ranges $\Delta\tau$, $\Delta\tau_{oct}$ reach their maximum in t_r and their values.

The stresses σ and τ are firstly calculated as functions of the plane angle θ:

$$\sigma(\theta)=\frac{\sigma_x}{2}+\frac{\sigma_x}{2}cos(2\theta)+\tau_{xy}\,sin(2\theta) \tag{3}$$

$$\tau(\theta)=-\frac{\sigma_x}{2}sin(2\theta)+\tau_{xy}\,cos(2\theta) \tag{4}$$

The principal normal stresses σ_1 and σ_2 are the solutions of the cubic equation, where $I_1(\theta)$, $I_2(\theta)$ and $I_3(\theta)$ are the three invariants of the stress tensor (equation (5)). The principal shear stress in the present case of plane stress will be computed according to equation (6).

$$\sigma^3-I_1(\theta)\cdot\sigma^2+I_2(\theta)\cdot\sigma-I_3(\theta)=0 \tag{5}$$

$$\tau_{12}(\theta)=\frac{|\sigma_1(\theta)-\sigma_2(\theta)|}{2} \tag{6}$$

The octahedral shear stress is determined with the following relation:

$$\tau_{oct}(\theta)=\frac{\sqrt{2}}{3}\sqrt{\sigma^2(\theta)+3\tau^2(\theta)} \tag{7}$$

The stress ranges of interest, i.e. $\Delta\tau$ and $\Delta\tau_{oct}$, are determined using an algorithm written for this purpose, as the example shows in Figure 5 a for $\Delta\tau_{max}$. The positions of the planes on which the above mentioned stresses and stress ranges reach their peak values ($\theta_{\sigma,max}$, $\theta_{\tau,max}$, $\theta_{\sigma1,max}$, $\theta_{\sigma2,max}$, $\theta_{\tau12,max}$, $\theta_{\tau oct,max}$, $\theta_{\Delta\tau,max}$, $\theta_{\Delta\tau oct,max}$) are all determined by algorithms written in MathCad, similar with the example given for $\theta_{\Delta\tau,max}$ in Figure 5 b.

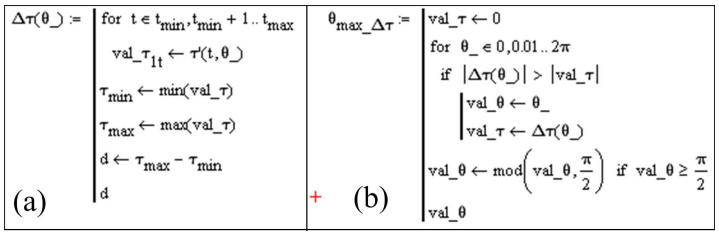

Fig. 5. Shear stress range calculation on plane θ (a) and plane position where the shear stress range is max (b).

3.5. Material characteristics used with the analyzed HCF models

The material properties which are used in the calculations are given in Table 3.

Table 3. Material properties.

Material	σ_{UTS} [MPa]	σ_{yield} [MPa]	σ_{-1} [MPa]	σ_0 [MPa]	τ_{-1} [MPa]
41Cr4	870	761	350	220	250

4. RESULTS AND DISCUSSION

The 11 HCF models reviewed in Chapter 2 were subjected to the CPOA assessment, each of them being applied for 14 load cases with different grades of nonproportionality. The obtained values for the stresses of interest and the angles of the planes where they are acting, are given in Table 4, for all the 11 models in 14 load cases.

Table 4. Obtained stress values, corresponding plane positions and CPOA for each model.

Parameter	Loading case													
	A1	**A2**	**A3**	**A4**	**A5**	**A6**	**A7**	**B1**	**B2**	**B3**	**B4**	**B5**	**B6**	**B7**
$\theta_{\sigma,max}$ [°]	44	135	133	135	135	135	135	0	0	0	-2	172	171	-10
σ_{max} [MPa]	240	-241	-242	-246	-250	-254	-259	240	240	240	-1	241	243	246
$\theta_{\tau,max}$ [°]	0	0	0	0	0	0	1	42	42	41	42	37	36	35
τ_{max} [MPa]	240	240	240	240	240	240	241	-120	-120	-120	-121	-121	-123	-126
$\theta_{\sigma1,max}$ [°]	15	17	17	16	17	16	18	0	0	0	0	0	0	0
$\sigma_{1,max}$ [MPa]	277	277	276	273	271	268	266	240	240	240	241	241	243	246
$\theta_{\sigma2,max}$ [°]	105	108	107	107	108	108	109	52	52	51	52	47	45	45
$\sigma_{2,max}$ [MPa]	-277	-278	-279	-281	-284	-287	-291	-80	-80	-80	-81	-81	-83	-86
$\theta_{\tau12,max}$ [°]	0	0	0	0	0	1	0	34	34	33	29	29	25	26
$\tau_{12,max}$ [MPa]	240	240	240	240	240	241	241	139	139	139	139	140	141	144
$\theta_{\tau oct,max}$ [°]	0	0	0	0	0	0	0	26	25	24	21	21	19	19
$\tau_{oct,max}$ [MPa]	196	196	196	196	196	196	197	120	120	120	120	121	122	124
$\theta_{\Delta\tau,max}$ [°]	87	88	87	88	0	0	0	53	53	52	51	50	46	44
$\Delta\tau_{max}$ [MPa]	422	422	421	421	420	420	420	223	222	220	217	214	211	210
$\theta_{\Delta\tau oct,max}$ [°]	85	87	1	2	1	89	6	38	36	30	29	24	22	16
$\Delta\tau_{oct,max}$ [MPa]	194	195	185	188	190	195	192	99	103	107	112	116	120	122
$\theta_{\sigma vM,max}$ [°]	0	0	0	0	0	0	1	29	29	27	23	25	21	21
$\sigma_{vM,max}$ [MPa]	416	416	416	416	416	417	418	255	255	255	255	257	259	263
$\sigma_{vM}(\theta_{\tau oct,max})$ [MPa]	416	416	416	416	416	417	417	254	254	254	253	256	258	262
CPOA(vM) [°]	0	0	0	0	0	0	1	3	3	3	2	3	2	2
$\theta_{\sigma vMs,max}$ [°]	0	0	0	0	0	0	1	29	29	27	23	25	21	21
$\sigma_{vMs,max}$ [MPa]	-416	-416	-416	-416	-416	-417	418	255	255	255	255	257	259	263
$\sigma_{vMs}(\theta_{\tau oct,max})$ [MPa]	-416	-416	-416	-416	-416	-417	417	254	254	254	253	256	258	262
CPOA(vMs) [°]	0	0	0	0	0	0	1	3	3	3	2	3	2	2
$\theta_{\sigma Tr,max}$ [°]	0	0	0	0	0	0	1	33	33	31	30	30	28	25
$\sigma_{Tr,max}$ [MPa]	480	480	480	480	480	481	482	277	277	277	278	280	283	287
$\sigma_{Tr}(\theta_{\tau oct,max})$ [MPa]	480	480	480	480	480	481	481	271	270	270	269	273	275	282
CPOA(Tr) [°]	0	0	0	0	0	0	1	7	7	7	9	9	9	6
$\theta_{\sigma Sin,max}$ [°]	64	N/A	N/A	N/A	N/A	N/A	N/A	174	N/A	N/A	N/A	N/A	N/A	N/A
$\sigma_{Sin,max}$ [MPa]	123	N/A	N/A	N/A	N/A	N/A	N/A	104	N/A	N/A	N/A	N/A	N/A	N/A
$\sigma_{Sin}(\theta_{\tau oct,max})$ [MPa]	88	N/A	N/A	N/A	N/A	N/A	N/A	98	N/A	N/A	N/A	N/A	N/A	N/A
CPOA(Sin) [°]	64	N/A	N/A	N/A	N/A	N/A	N/A	148	N/A	N/A	N/A	N/A	N/A	N/A
$\theta_{\sigma Yok,max}$ [°]	24	115	115	115	115	115	117	158	157	158	155	155	151	149
$\sigma_{Yok,max}$ [MPa]	375	-376	-378	-382	-387	-392	-399	331	331	332	332	334	336	340
$\sigma_{Yok}(\theta_{\tau,max})$ [MPa]	240	239	234	226	217	206	207	38	36	37	23	40	37	26
CPOA(Yok) [°]	24	115	115	115	115	115	116	115	115	117	113	117	116	114
$\theta_{\sigma Fin,max}$ [°]	79	79	81	81	82	81	81	59	57	56	56	56	52	49
$\sigma_{Fin,max}$ [MPa]	220	220	220	219	218	216	215	123	125	124	121	116	118	118
$\sigma_{Fin}(\theta_{\sigma Fin,max})$ [MPa]	220	220	220	219	218	216	215	123	125	124	121	116	118	118
CPOA(Fin) [°]	0	0	0	0	0	0	0	0	0	0	0	0	0	0
$\theta_{\sigma Mat,max}$ [°]	79	79	81	81	82	81	81	149	147	148	148	143	142	138
$\sigma_{Mat,max}$ [MPa]	220	220	220	219	218	216	215	146	145	145	144	142	141	140
$\sigma_{Mat}(\theta_{\Delta\tau,max})$ [MPa]	216	215	216	214	210	210	210	128	128	127	126	124	124	124
CPOA(Mat) [°]	8	9	6	7	82	81	81	96	94	96	97	93	95	95
$\theta_{\sigma McD,max}$ [°]	84	84	83	84	84	87	85	146	144	143	142	142	138	137
$\sigma_{McD,max}$ [MPa]	214	214	213	213	212	212	211	126	125	124	123	122	120	120
$\sigma_{McD}(\theta_{\Delta\tau,max})$ [MPa]	213	212	213	212	210	210	210	119	118	117	116	114	113	113
CPOA(McD) [°]	3	3	3	3	84	87	85	92	91	91	91	92	91	93
$\theta_{\sigma SinII,max}$ [°]	0	0	175	0	0	175	0	57	38	36	33	32	28	28
$\sigma_{SinII,max}$ [MPa]	120	123	126	128	129	130	131	69	69	71	73	75	76	77
$\sigma_{SinII}(\theta_{\Delta\tau oct,max})$ [MPa]	117	118	125	127	129	119	128	66	68	68	71	72	73	72
CPOA(SinII) [°]	85	87	174	2	1	87	6	19	2	6	4	8	6	11
$\theta_{\sigma Cro,max}$ [°]	85	82	82	92	90	98	96	28	24	147	19	13	14	3
$\sigma_{Cro,max}$ [MPa]	122	121	121	121	120	122	122	71	74	78	81	84	87	88
$\sigma_{Cro}(\theta_{\Delta\tau oct,max})$ [MPa]	122	121	113	116	117	120	119	70	73	77	80	84	86	88
CPOA(Cro) [°]	0	5	81	90	89	9	90	10	12	117	10	11	8	13
$\theta_{\sigma KK,max}$ [°]	90	90	90	90	90	90	90	74	123	121	120	122	115	113
$\sigma_{KK,max}$ [MPa]	118	119	120	118	119	119	118	43	45	46	47	49	49	50
$\sigma_{KK}(\theta_{\Delta\tau vM,max})$ [MPa]	106	111	97	96	101	117	97	5	6	4	8	8	12	11
CPOA(KK) [°]	5	3	89	88	89	1	84	36	87	91	91	98	93	97

where:
$\sigma_{XX}(\theta_{\sigma YY,max})$ – the equivalent stress corresponding to model XX, on the plane θ considered to be critical where the stress σ_{YY} reaches a maximum value;

CPOA(XX) – the CPOA of the model XX

vM – von Mises;
vMs – Signed von Mises;
Tr – Tresca;
Sin – Sines;
Yok – Yokobori;
Fin – Findley;
Mat – Matake;
McD – McDiarmid;
SinII – Sines (II);
Cro – Crossland;
KK – Kakuno-Kawada;

The following figures (Figure 6 - 16) present the evolution of the selected 11 HCF models in 6 of the 14 loading cases, by plotting on an angular hodograph two stress quantities in t_r as functions of the plane angle θ: the equivalent stress and the stress defining the critical plane (see Table 1). The variation of CPOA for the different phase shift angles in case of each model is also presented in the figures.

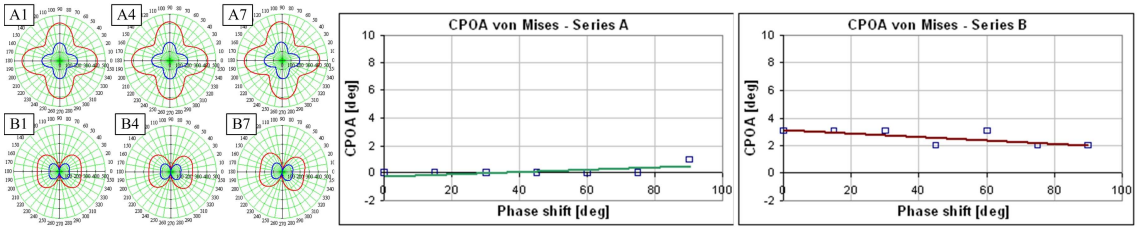

Fig. 6. CPOA for the von Mises model.

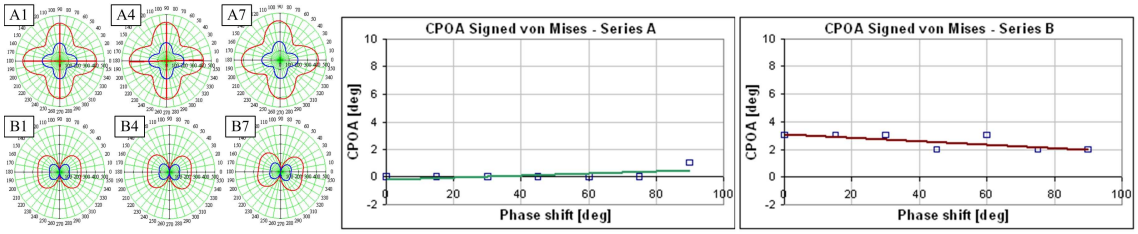

Fig. 7. CPOA for the Signed von Mises model.

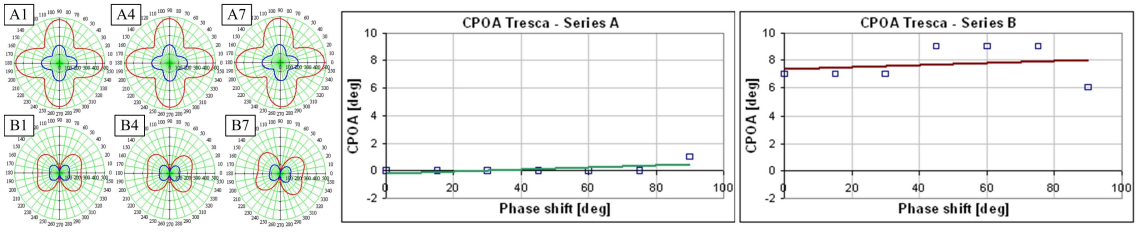

Fig. 8. CPOA for the Tresca model.

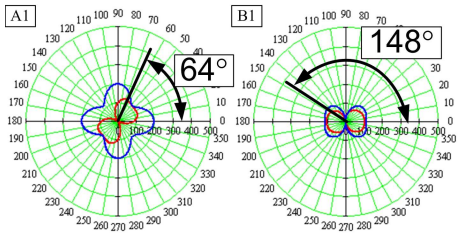

Fig. 9. CPOA for the Sines model.

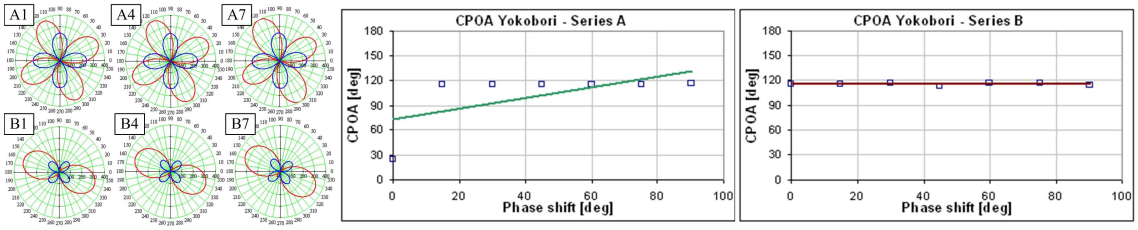

Fig. 10. CPOA for the Yokobori model.

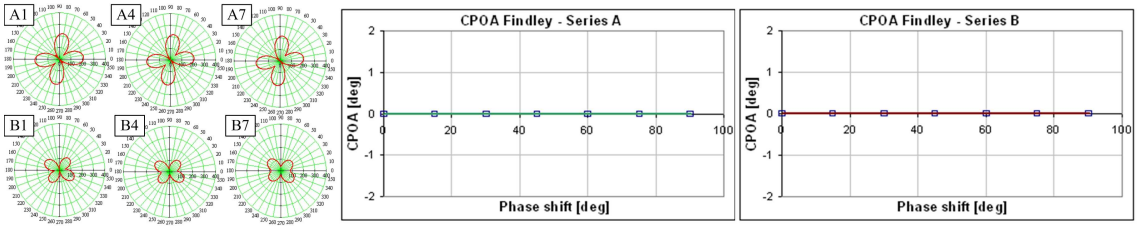

Fig. 11. CPOA for the Findley model.

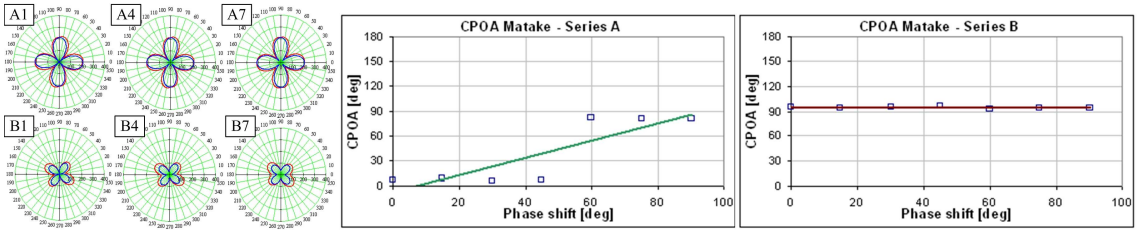

Fig. 12. CPOA for the Matake model.

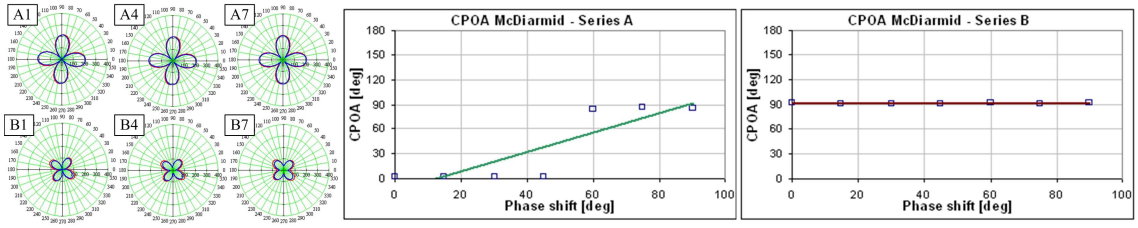

Fig. 13. CPOA for the McDiarmid model.

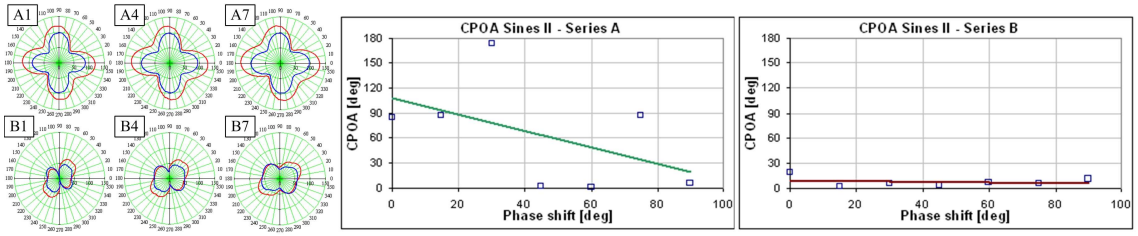

Fig. 14. CPOA for the Sines (II) model.

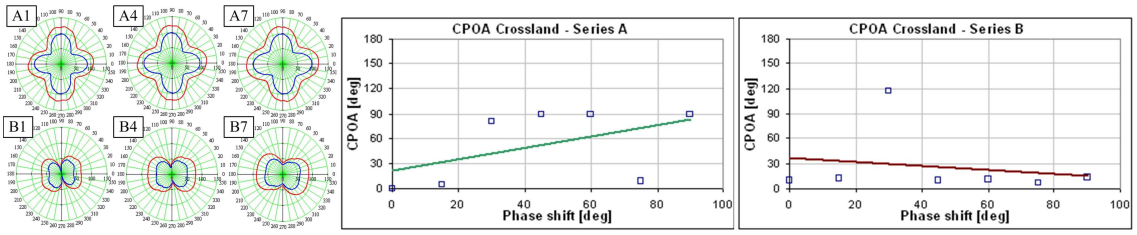

Fig. 15. CPOA for the Crossland model.

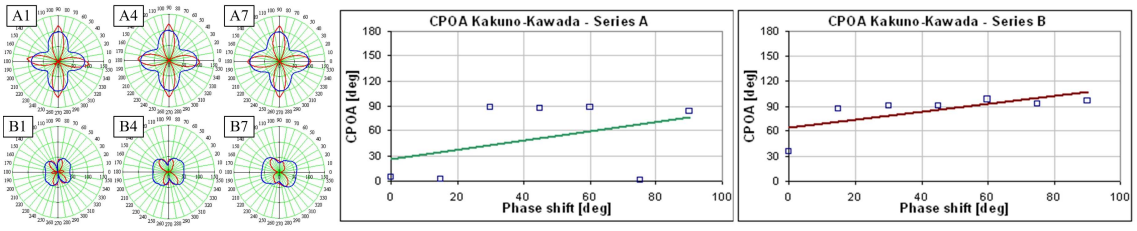

Fig. 16. CPOA for the Kakuno-Kawada model.

As Figures 6-16 show, the CPOA has various graphs depending on the model. The equivalent stress models (i.e. von Mises (Figure 6), Signed von Mises (Figure 7) and Tresca (Figure 8)) give a rather weak influence of the phase shift on the CPOA. In all the 3 cases, the CPOA value remains in the range between -2° and 10°. In case of the von Mises and Signed von Mises model, a slightly descending tendency of CPOA can be observed with the increasing phase shift. However, the Tresca model's CPOA shows an ascending tendency with the increasing phase shift and a larger scatter. It is also important to mention that all three models generate CPOA values close to zero when applied to Series A from the analyzed loading cases, while in case of Series B, the CPOA values are above-zero.

The Sines model (Figure 9) was applied only for the two proportional loading cases, and even so it generated high values for CPOA, meaning large position difference between the plane of maximum stress and the critical plane.

As expected, the critical plane models (Figures 10-13) have proven to be less predictable then the equivalent stress models. The values of CPOA generally jump between 0° and 90°. While the Yokobori model (Figure 10) generates almost constant CPOA values at 90°, the Findley model (Figure 11) by definition gives the best result: CPOA = 0°, since the critical plane and the plane of maximum stress are defined to be identical. As for the Matake (Figure 12) and McDiarmid (Figure 13) models, both give similar results. In Series A, both models give CPOA values which jump between approx. 0° and 90°, the shift apparently happening at 60°. In case of Series B, both models give stable, around 90° for CPOA. The Matake model gives slightly higher CPOA values then the McDiarmid model, due to the difference in material constants used.

According to this study, the models based on stress invariants (Figures 14-16) give the worst results in terms of CPOA from the analyzed 11 models. It can be seen once again that the scatter is much higher for Series A than for Series B. In case of the Sines (II) model (Figure 14) it is of 180°, which can be due to inconsistencies in defining the amplitude of the second invariant of the stress deviator, analyzed in another work [19]. However, for Series B the Sines (II) model gives an almost constant CPOA of around 6° for all the analyzed grades of nonproportionality. The finding is similar in case of the Crossland (Figure 15) and Kakuno-Kawada (Figure 16) models too. However, it can be observed that for Series B the Kakuno-Kawada model predicts CPOA to be around 90°, while the Sines (II) and Crossland models floor it to 0°.

It can be observed that the majority of the models are more stable in terms of CPOA in case of the loadings from Series B, where the dominant stress is the normal stress. In case of Series A, where the dominant stress is the shear stress, the scatter among CPOA values is much wider. The exceptions from this tendency are the von Mises, Signed von Mises, Tresca, Sines and Findley models. The latter gives absolute 0 values for CPOA, while the Sines model is not defined for nonproportional multiaxial loadings.

4. CONCLUSIONS

A number of 11 multiaxial HCF models are reviewed and analyzed in this paper, based on a parameter defined as the difference angle between the positions of the critical plane and the plane where the equivalent stress reaches its maximum. This parameter, denoted as the Critical Position Offset Angle – CPOA, can be considered as a measure for the accuracy of the model. Thus, the less CPOA is, the better defined the model. The models are applied for 14 simulated loadings with different grades of nonproportionality, given by various phase shift angles between the normal and shear stress cycle.

It is found that the models generate higher CPOA values with wider scatter in case of loadings with dominant shear stress. Furthermore, the models based on the second invariant of the stress deviator (Sines (II), Crossland, Kakuno-Kawada) give higher CPOA values than the equivalent stress models (von Mises, Signed von Mises, Tresca). This may be explained by inconsistent definition of the mentioned invariant in case of nonproportional loading. The CPOA assessment applied for the Findley model always produces zero values, given by the model's definition. As a result of this, the CPOA assessment is not a valid measure of the Findley model's accuracy. Furthermore, the Sines model is not defined for nonproportional loadings, thus plotting the variation of CPOA with the phase shift angle is not applicable.

Given the above and taking into account the mentioned exceptions, the CPOA assessment is aimed to be an additional tool in selecting the HCF models for a durability evaluation, by predicting the difference between the plane of maximum equivalent stress and the critical plane. This can be useful in applying the appropriate HCF model for the given case of loading.

ACKNOWLEDGMENT

This work was partially supported by the strategic grant POSDRU/88/1.5/S/50783, Project ID50783 (2009), co-financed by the European Social Fund – Investing in People, within the Sectorial Operational Programme Human Resources Development 2007-2013.

REFERENCES

[1] Feng, J., Titus, P., Proposed Method for Evaluating Multiaxial Fatigue in ITER, PSFC/RR-07-4, Plasma Science and Fusion Center MIT, Cambridge, U.S.A., 2007.
[2] Karolczuk, A., Macha, E., A review of critical plane orientations in multiaxial fatigue failure criteria of metallic materials, International Journal of Fracture, vol. 134, no. 3-4, 2005, p. 267-304.
[3] Dumitru, I., Kun, L., On the multiaxial high cycle damage parameters, Bulletin of the Petroleum-Gas University of Ploiesti – Technical Series, vol. LXIII, no. 1, 2011, p. 117-126.
[4] Socie, D., Marquis, G., Multiaxial Fatigue, Society of Automotive Engineering International, Inc. Warrendale, Pa, 2000.
[5] Wang, Y.Y., Yao, W.X., Evaluation and comparison of several multiaxial fatigue criteria, International Journal of Fatigue, vol. 26, 2004, p. 17-25.
[6] Ninic, D., Stark, H.L., A multiaxial fatigue damage function, International Journal of Fatigue, vol. 29, 2007, p. 533-548.
[7] Von Mises, R., Mechanik der festen Körper im plastisch deformablen Zustand, Nachrichten von der Gesellschaft der Wissenschaften zu Göttingen, Mathematisch-Physikalische Klasse, vol. 1, 1913, p. 582–592.
[8] Bishop, N.W.M., Sherrat, F., Finite element based fatigue calculations, NAFEMS: The International Association for the Engineering Analysis Community, Farnham, U.K., 2000.
[9] Tresca, H., Mémoire sur l'écoulement des corps solides soumis à de fortes pressions, Comptes Rendus Hebdomadaires des Seances de l'Academie des Sciences Paris, vol. 59, 1864, p. 754.
[10] Sines, G., Failure of materials under combined repeated stresses with superimposed static stresses, Technical Note 3495, National Advisory Committee for Aeronautics, Washington DC, U.S.A., 1955.
[11] Yokobori, T., Yoshimura, T., A criterion for fatigue fracture under multiaxial alternating stress state, Report 2, 1966, Tohoku University, Sendai, Japan, p. 45-54.
[12] Findley, W.N., Fatigue of metals under combinations of stresses, Transactions of A.S.M.E., vol. 79, 1957, p. 1337-1348.
[13] Matake, T., An explanation on fatigue limit under combined stress, Bulletin of Japan Society Mechanical Engineering, vol. 20, no. 141, 1977, p. 257-263.

[14] McDiarmid, D.L., A shear stress based critical-plane criterion for multiaxial fatigue failure for design and life prediction, Fatigue & Fracture of Engineering Materials & Structures, vol. 17, no. 12, 1994, p. 1475-1485.
[15] Crossland, B., Effect of large hydrostatic pressures on the torsional fatigue strength of an alloy steel, Proceedings of the International Conference on Fatigue of Metals, ImechE London, U.K., 1956, p. 138-149.
[16] Sines, G., Behavior of metals under complex static and alternating stresses, Metal Fatigue, McGraw-Hill, New York, 1959, p. 145-169.
[17] Kakuno, H., Kawada, Y., A new criterion of fatigue strength of a round bar subjected to combined static and repeated bending and torsion, Fatigue & Fracture of Engineering Materials & Structures, vol. 2, 1979, p. 229-236.
[18] Kun, L., Neş, C.S., Dumitru, I., Faur, N., Durability Study of a Machine Shaft Based on the Material Behavior of 41Cr4 Steel Subjected to Rotating Bending, Solid State Phenomena, vol. 188 – Advanced Materials and Structures IV, Eds: Nicoară, M., Răduță, A., Opriş C., 2012, p. 256-261.
[19] Kun, L., Dumitru, I., Cotuna, E., A study on multiaxial high cycle fatigue models, Proceedings of The 15th International Conference Modern Technologies, Quality and Innovation ModTech2011 – New Face of T.M.C.R., Chişinău, Republic of Moldova, vol. I, 2011, p. 561-564.